The Astrophysical Journal, 581:276–284, 2002 December 10

FORMATION OF MOLECULAR HYDROGEN ON AMORPHOUS WATER ICE: INFLUENCE OF MORPHOLOGY AND ULTRAVIOLET EXPOSURE

J. E. Roser,[1] G. Manicò,[1,2] V. Pirronello,[2] and G. Vidali[1]

Received 2002 April 26; accepted 2002 August 14

ABSTRACT

In this paper, we report on the formation of molecular hydrogen on different types of amorphous water ice. We show that mass spectra of desorbing molecules upon formation are sensitive to the way in which ice is deposited on a cold substrate, to its thermal history, and to the action of UV photons. Implications that these results bear on H_2 formation in dense quiescent clouds are presented and discussed.

Subject headings: astrochemistry — dust, extinction — ISM: molecules — methods: laboratory — molecular processes

1. INTRODUCTION

The formation of the hydrogen molecule, the most abundant in the universe, is one of the fundamental processes occurring in the interstellar medium. It has been recognized that it cannot form efficiently in the gas phase, because upon formation the release of the energy excess via radiative decay is not allowed by selection rules, and that the role of dust grains as catalysts is crucial to explain its abundance. However, the dynamics and the rate of formation of H_2 molecules on the surface of grains are not completely clear yet.

After the pioneering theoretical calculations of Hollenbach & Salpeter (1971) and Hollenbach, Werner, & Salpeter (1971), the problem of H_2 formation on interstellar grains has been taken up by several authors (see, e.g., Pirronello et al. 2000 and references therein).

In his theoretical work, Smoluchowski (1979, 1981, 1983) questioned the choice of a crystalline structure for the grain and considered the formation of H_2 on amorphous surfaces, obtaining a reduced formation efficiency. This stimulated some authors to propose alternative mechanisms of formation (Pirronello & Averna 1988; Averna & Pirronello 1991; Watanabe, Horii, & Kouchi 2000). Recently, new experimental results gave further insight into the understanding of the problem of H_2 formation on surfaces of silicates and amorphous carbon, which are good analogs of grains in diffuse clouds (Pirronello et al. 1997a, 1997b; Vidali et al. 1998; Pirronello et al. 1999) and of icy mantles accreted on them in dense clouds (Manicò et al. 2001).

In this paper, we consider the formation of molecular hydrogen on pure water ice surfaces. Actually, at least three types of interstellar ice can be distinguished (Schutte 1999): type I contains mostly H_2O, type II is a methanol-rich ice, and type III is apolar ice containing a higher abundance of molecules, such as CO. Water ice is by far the most abundant and the best-studied component of interstellar ice.

Research on water ice in space was stimulated by the early detection of the absorption band at ~ 3 μm toward the embedded protostellar BN object (Gillett & Forrest 1973; Gillett et al. 1975). Laboratory experiments in which water vapor was deposited onto inert surfaces at temperatures less than ~ 30 K showed that this observed band is best fitted by the OH-stretch vibration band of impure water ice (Hagen, Tielens, & Greenberg 1981; Schmitt, Greenberg, & Grim 1989).

The slow process of accretion of molecules from the gas phase produces, in laboratory experiments, an amorphous solid structure (Rice 1975; Narten, Vencatesh, & Rice 1976). Léger et al. (1979) and Hagen et al. (1981) compared laboratory infrared spectra of amorphous water ice deposited at ~ 10 K with observed interstellar features of water ice mantles, providing evidence that in interstellar conditions, water ice mantles are mainly amorphous, with a structure that is microporous in nature (Mayer & Pletzer 1986). From the analysis of the 3.07 μm band profile toward the Taurus molecular cloud, Jones & Williams (1984) concluded that ice is produced by the reaction of accreted OH with H, as originally proposed by van de Hulst (1949).

Several different phases of water ice obtained by vapor deposition have been reported in the literature. The established forms, obtained with pure water at low pressure, are two crystalline phases, namely, the hexagonal and cubic polymorphs, and a number of amorphous phases (Li & Jenniskens 1997). The most commonly studied amorphous form is the low-density amorphous water ice, which has a local density of 0.94 ± 0.03 g cm^{-3} and can be obtained by depositing water vapor on an inert surface at 77 K (Narten et al. 1976; Mayer & Pletzer 1986).

Vichnevetski, Bass, & Sanche (2000) experimentally studied morphological differences between amorphous water ice film and a crystalline one. They measured the electron-stimulated desorption of metastable molecular nitrogen from N_2 condensed on it and related the variation of the signal detected to the variation in density of N_2 molecules at the surface of a porous water film. They deposited a water ice film at 20 K, obtaining an amorphous water ice sample, and showed that this structure contains many pores that greatly increase the effective surface area of the film. Molecules adsorbed on such a structure, such as N_2 or H_2, diffuse into these micropores, which have diameters in the range ~ 15–20 Å (Langel et al. 1994; Mayer & Pletzer 1986), and throughout the film, ensuring a near-uniform distribution of molecules over the large effective surface of the film.

[1] Physics Department, Syracuse University, 201 Physics Building, Syracuse, NY 13244-1130; jeroser@syr.edu, gvidali@syr.edu.

[2] Dipartimento di Metodologie Fisiche e Chimiche per l'Ingegneria, Università di Catania, Viale Doria 6, 95125 Catania, Sicily, Italy; gmanico@dmfci.unict.it, vpirrone@dmfci.unict.it.

Interaction of H_2 molecules with microporous ice and, in particular, the incorporation rate at $\sim$10 K have been examined by Rowland, Fisher, & Devlin (1991). They found that, in contrast to N_2, the H_2 mobility at the ice-H_2 (g) interface is sufficient at $\sim$10 K for H_2 to become enclosed in the ice micropores.

A different high-density (1.1 ± 0.1 g cm^{-3}) amorphous form was first obtained by Narten et al. (1976) by depositing water vapor at $\sim$10 K. Their X-ray diffraction experiments showed that the increased density of this form of ice, with respect to the lower density amorphous ice, was due to the presence of water molecules at distances between those of the first and second nearest neighbor at the interstitial site of the solid structure. This high-density amorphous ice is potentially important in astrophysics, because infrared spectra of water vapor deposited on low-temperature substrates provide the best fit to the 3.07 μm ice band (Jenniskens et al. 1995).

Experiments performed after Narten et al. (1976) failed to reproduce the high-density form on substrates other than single-crystal copper (see references in Jenniskens et al. 1995), until Heide (1984) showed that high-density ice also forms by vapor deposition on amorphous carbon films. Jenniskens & Blake (1994), in their selected area electron diffraction study, obtained patterns identical to those reported by Heide (1984), confirming the formation of a high-density amorphous form when water vapor is deposited on an amorphous carbon film at $\sim$15 K, and concluded that this form of ice is not an artifact of epitaxial growth on an oriented single-crystal surface, as had been previously suggested (Jenniskens & Blake 1994).

High-density amorphous water ice also can be prepared in a different way from vapor deposition. Mishima, Calvert, & Whalley (1984) discovered that an ice crystal can be transformed by pressure into a high-density amorphous phase, and their work was followed by other examples of pressure-induced amorphization (Mishima 1996 and references therein). The phenomenon of the pressure-induced phase transition from crystalline to amorphous ice has been studied by Tse (1992) with constant-pressure molecular dynamics calculations. He proposed that the physical mechanism underlying the conversion of the high-density amorphous form from the crystalline one is the collapse of water molecules into the empty cages in the crystalline structure. Tse (1992) also argued that pressure-induced amorphous ice has more hexagonal order than the vapor-deposited amorphous form. Formation of a very high density amorphous water ice at a pressure of 1 bar and a temperature of 77 K recently has been reported (Loerting et al. 2001). Amorphization of crystalline forms by means of electron or ion bombardment also has been reported (Heide 1984; Heide & Zeitler 1985; Hudson & Donn 1991).

Changes in the structure of water ice due to irradiation with photons are also reported in the literature. Kouchi & Kuroda (1990) studied the effect of ultraviolet radiation on water ice by means of in situ reflection electron diffraction. Following the structural changes taking place in the sample, they found that, below $\sim$70 K, photons from a deuterium lamp ($\leq\sim$11.3 eV) transform cubic ice into amorphous ice. They also inferred that other high-energy particles should amorphize ice crystals below $\sim$70 K and concluded that crystalline ice in some interstellar environments (like stellar atmospheres, asteroids, and planetary satellites) should be rendered amorphous by UV radiation in times short compared with the timescale of stellar evolution. However, the dose of 3×10^{13} photons cm^{-2} at $\sim$10 K reported by Kouchi & Kuroda (1990) is less than 6×10^{-5} photons per water molecule, given a penetration depth of $\sim$0.15 μm at 120 nm (Okabe 1978). This is a strikingly low value, suggesting that the conversion from one form to another would need further attention (Jenniskens et al. 1995).

High-density amorphous ice may be transformed into the low-density form by raising the temperature of the sample. During the warm-up of the water ice sample from 15 to $\sim$188 K, Jenniskens & Blake (1994) observed a progression of three amorphous forms of water ice with well-defined transitions. The thermal transition from the high-density form to the more familiar low-density amorphous form occurs gradually over the range of temperature between 38 and $\sim$68 K. By raising the temperature further up to $\sim$131 K, the ice transforms into a third amorphous form that coexists with cubic crystals for at least 16 hr at $\sim$178 K (Jenniskens & Blake 1994). Transition from the high- to low-density form is irreversible, but low-density ice can be transformed back to high-density ice if the sample is irradiated with an intense electron beam when it is cooled below $\sim$70 K (Heide 1984).

In this paper, we give further insight into the topic of the formation of molecular hydrogen at $\sim$10 K on surfaces of different types of amorphous water ice: high density, low density, and UV irradiated. After exposing such surfaces to H and D atomic beams, we perform a temperature-programmed desorption (TPD) by raising the substrate temperature, monitoring in situ the formation of hydrogen deuterium (HD) by mass spectrometry. The shape, position, and intensity of the TPD spectra are strongly affected by the structure of the ice, probably through relevant changes in the distribution and the size of the micropores embedded in the amorphous layer.

2. EXPERIMENTAL PROCEDURES

The experimental apparatus and techniques used in this study are essentially the same as the ones described in detail elsewhere (Pirronello et al. 1997b, 2000; Vidali et al. 1998; Manicò et al. 2001). The apparatus consists of two triply differentially pumped beam lines, one for H and the other for D (see Fig. 1). Atomic H and D beams at thermal energy are produced by feeding 50 W of radio-frequency power into each of two cavities containing water-cooled Pyrex envelopes filled with high-purity molecular HD gas. The dissociation efficiency, measured with a quadrupole mass spectrometer located in the main ultrahigh vacuum (UHV) chamber, is routinely around 80% for D_2 and 90% for H_2 and stable during the runs. The use of two beams allows, as explained in detail elsewhere (Vidali et al. 1998), the detection of the formation of HD with unprecedented sensitivity, thus bypassing the limitations of using one source. The estimated atom flux is comparable to the one used in previous work. A tiny fraction of Lyα UV photons generated in the sources can reach the target. We calculated that, in the extreme case in which the whole input power is converted into Lyα photons, less than 1 photon per 1000 hydrogen atoms is absorbed in the first few ice monolayers.

The sample and detector (a quadrupole mass spectrometer) are placed in a stainless steel chamber pumped by an ion pump, a turbomolecular pump, and, occasionally, by a titanium sublimation pump. The chamber is kept at a pressure

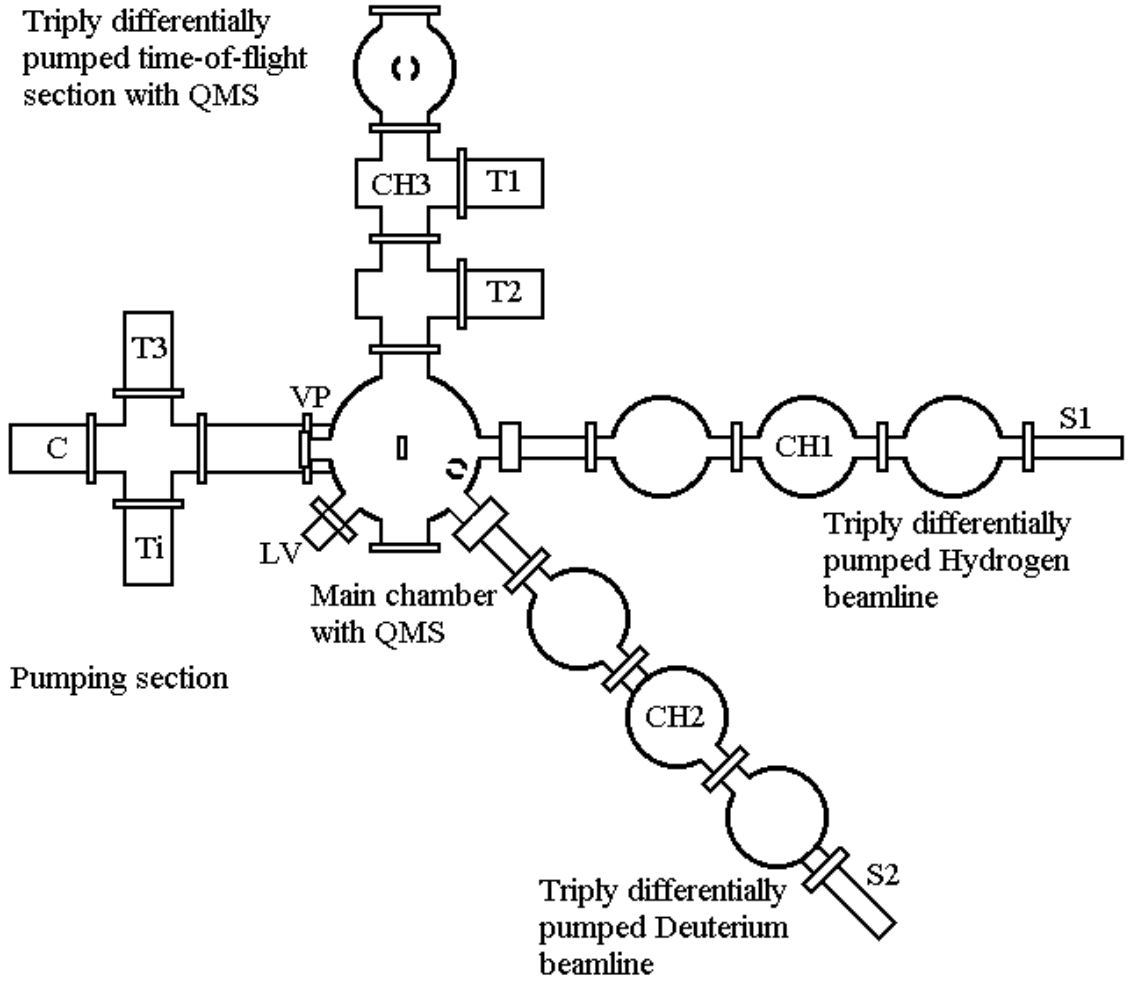

FIG. 1.—Schematic of the apparatus—top view. S1 and S2 denote H_2 and D_2 radio-frequency dissociation sources; CH1, CH2, and CH3 denote the positions of mechanical choppers; T1, T2, and T3 are turbopumps, while Ti is a titanium sublimation pump and C a cryopump; LV is the leak valve for introducing water vapor into the system through a capillary; and VP is the MgF_2 viewport for admitting UV light into the system.

in the mid-10^{-10} torr range during measurements. The sample is placed on a copper holder in thermal contact with a Helitrans continuous flow UHV-compatible cryostat. The holder terminates in a thin slab that holds the sample on one side and a ceramic (Mycor) box on the other. The ceramic box contains a heater made of turns of constantan wire. To ensure a good thermal contact between the sample (in this case, a copper disk in which a film of water ice is grown) and the copper slab, a thin film of indium is inserted. The thermometer, a calibrated silicon diode, is housed in a small cavity behind the sample; this cavity is filled with indium for good thermal contact. The sample holder is surrounded by a thermal shield anchored to an upper stage of the cryostat.

The temperature of the sample can be changed by using the heater or, in thermal desorption experiments when a high heating rate of the sample is required, by shutting off the flow of liquid helium in the continuous flow cryostat. The temperature rise of the sample versus time obtained with this method is very reproducible, but it is not linear over the whole range of temperature (10–40 K) employed in these experiments.

The ice sample is prepared by lowering the sample to a position 1 cm in front of a capillary to allow water vapor to be directly deposited onto the copper disk. A measured quantity of water vapor is admitted into the chamber through a heated stainless steel manifold and a UHV leak valve. Before deposition, the deionized water undergoes repeated cycles of freezing and thawing to remove trapped gases. The sample is held at 10 K or lower during deposition and the deposition rate is $\sim$8 layers s^{-1}, for a total thickness of the order of 1200 layers. This method of preparing the ice sample should produce a high-density amorphous water ice (Stevenson et al. 1999). Although realistic interstellar ice also contains molecules such as CO, CO_2, or CH_3OH (Whittet 1997), we decided to concentrate our work on the study of pure water ice in order to be in a better defined experimental condition.

The ice sample is periodically removed and redeposited with excellent reproducibility of results. As described in the previous section, it has been reported (Jenniskens & Blake 1994; Jenniskens et al. 1995) that a gradual change from high-density to low-density amorphous ice occurs at a temperature in the 38–70 K range. In the study of high-density amorphous ice, we always kept the ice sample below 38 K. To study the formation of molecular hydrogen on low-density amorphous ice, after deposition at 10 K, we gradually heated the high-density ice to 90 K and held the temperature at that value for at least 5 minutes. Then the sample was cooled down to $\sim$10 K. A third method for preparing the ice sample consists of filling the UHV chamber

with water vapor via the capillary with the sample in the raised position to prevent water vapor from being directly deposited onto the copper disk. The ice layer then forms by the sticking of H_2O molecules on the sample from random directions from the gas phase. These last two procedures gave similar ices, as judged by the similar signatures of the thermal desorption spectra (see below). Most of our data on low-density amorphous ice were taken on an ice film made using the first method, i.e., by gradual heating of ice deposited at 10 K.

H and D beams aimed at the sample were admitted into the chamber for a fixed amount of time. A thermal programmed desorption was performed, and the number of HD molecules leaving the sample was recorded with the quadrupole mass spectrometer. The TPD experiment, in which the temperature of the sample is increased at an initial average rate of $\sim$1 K s^{-1}, essentially accelerates any thermally activated processes that, in real interstellar conditions, would take too long to be reproduced in the laboratory.

The shape of the TPD signal reflects the kinetics of formation on/ejection from the surface of the molecule, while the temperature values at which there is a desorption feature, such as a maximum or a shoulder in a desorption rate trace, give information on the energetics of the processes leading to desorption. However, the raw traces that are shown below must be analyzed in order to account for effects (such as the heating rate or the pumping speed and geometric configuration of the apparatus) that might influence the value of the temperature at which a certain feature is seen as well as the shape of the tails of the peaks. An analysis to extract the physically meaningful parameters, such as the characteristic energies for the process of diffusion, recombination, and desorption, is given in § 4.

To make sure that no memory effects were present because of evolution of gases from the bulk of the sample or from deposition of background gas onto the surface, frequent "control runs" were performed; in these cases, no atomic hydrogen was admitted before we proceeded to execute the experiment as described below. No trace of HD formed on the sample was detected under these conditions.

In our previous investigation of molecular hydrogen formation on high-density amorphous ice, we saw that there was not a great difference in the recombination efficiency using cooled ($\sim$200 K) or room temperature atomic beams (Manicò et al. 2001). Thus, in this investigation, in order to avoid technical complications, we employed room temperature beams.

Both low-density and high-density amorphous water ice samples were irradiated with UV photons prior to the exposure to H and D beams. UV light was produced using a Perkin-Elmer Optoelectronics short-arc Xe flash lamp (model FX-1155) located outside the main chamber. The light was focused using a MgF_2 plano-convex lens and sent onto the sample via a MgF_2 viewport. The radiation covered the whole area of the sample. We estimate the total flux of UV radiation with wavelengths below 350 nm to be 5 mW over a sample area of 1 cm^2, or 6×10^{15} photons s^{-1} cm^{-2}, assuming an average UV photon of wavelength of 225 nm.

3. RESULTS

In Figure 2, we report the total HD yield obtained from experiments using H and D beams as a function of the atomic beams' irradiation time on low-density amorphous ice at the sample temperature of 10.5 K. The raw yield of HD is corrected for the instrument response and for the probabilities to different reaction paths yielding H_2 and D_2. The fact that for both low-density and high-density ice the yield versus exposure does not show any saturation behavior (Manicò et al. 2001) indicates that the coverage of H and D adatoms is in a submonolayer regime, which is exactly what is desired for astrophysical applications.

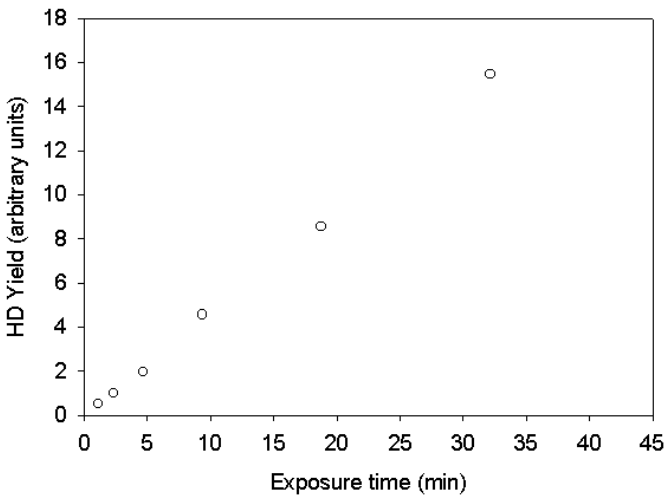

FIG. 2.—HD yield vs. exposure time of the sample to H and D for low-density amorphous ice. The sample adsorption temperature is $\sim$10.5 K.

Figure 3 shows the recombination efficiency on low-density amorphous ice (obtained with the two preparation methods described in the previous section) and high-density amorphous ice as a function of the temperature at which the sample was irradiated with H and D atoms. The recombination efficiency is given by the HD yield in a temperature-programmed experiment divided by half of the H and D beam fluence and corrected for the instrument response

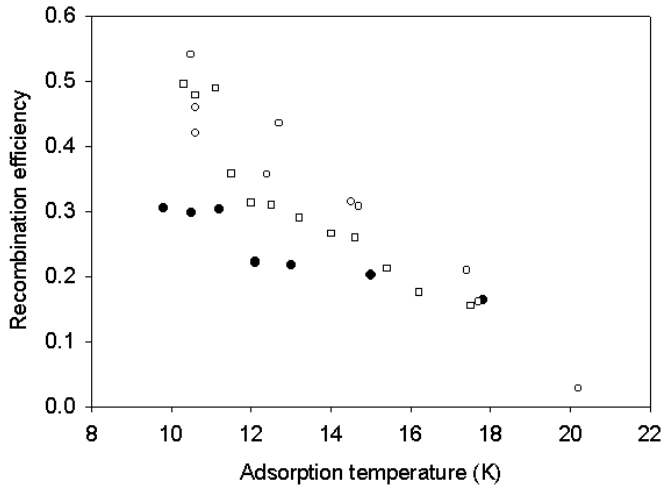

FIG. 3.—Recombination efficiency of molecular hydrogen vs. sample temperature of H atoms. Filled circles are for high-density amorphous ice (Manicò et al. 2001), open circles are for low-density amorphous ice prepared by heating high-density amorphous ice, and open squares are for water vapor–deposited low-density amorphous ice. The error bars are comparable to the size of the symbols. The scatter in the data points reflects the variability in the ice preparation methods.

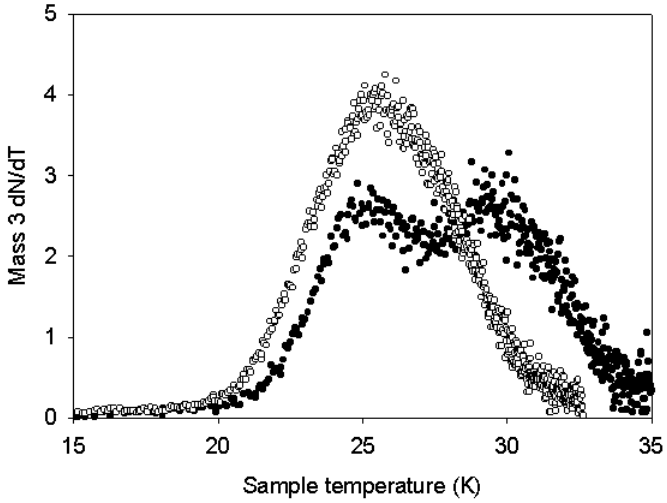

FIG. 4.—Desorption rate (dN_{HD}/dT) vs. ramp temperature after adsorption of H and D for 4 minutes on high-density amorphous water ice at ~10 K before (*filled circles*) and after (*open circles*) UV exposure for 15 minutes. Traces have been scaled to yield the same area.

function and for the probability of different reaction paths. The data for high-density amorphous ice are from Manicò et al. (2001).

Figures 4 and 5 show how UV irradiation of, respectively, high-density and low-density amorphous ice influences the shapes of the TPD traces, indicating that the UV radiation affects the morphology of the ice. Changes in the morphology are reflected quantitatively in the values of the activation energy of the $H_{surface} + D_{surface} \rightarrow HD$, as explained in § 4.

4. ANALYSIS

The features of thermal desorption traces, such as the ones presented in Figure 6, contain information on the energetics of the processes of diffusion, recombination, and desorption of species from the surface of the sample. In previous experiments, characteristic changes in the traces for samples exposed to H and D for progressively longer times

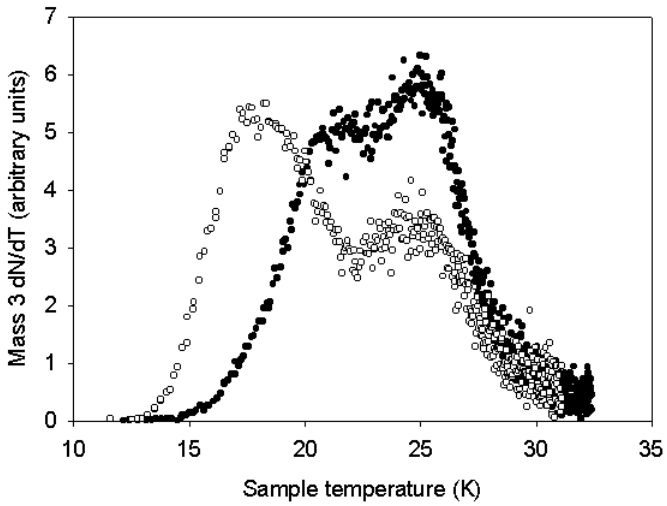

FIG. 5.—Same as in Fig. 4, except for low-density amorphous ice

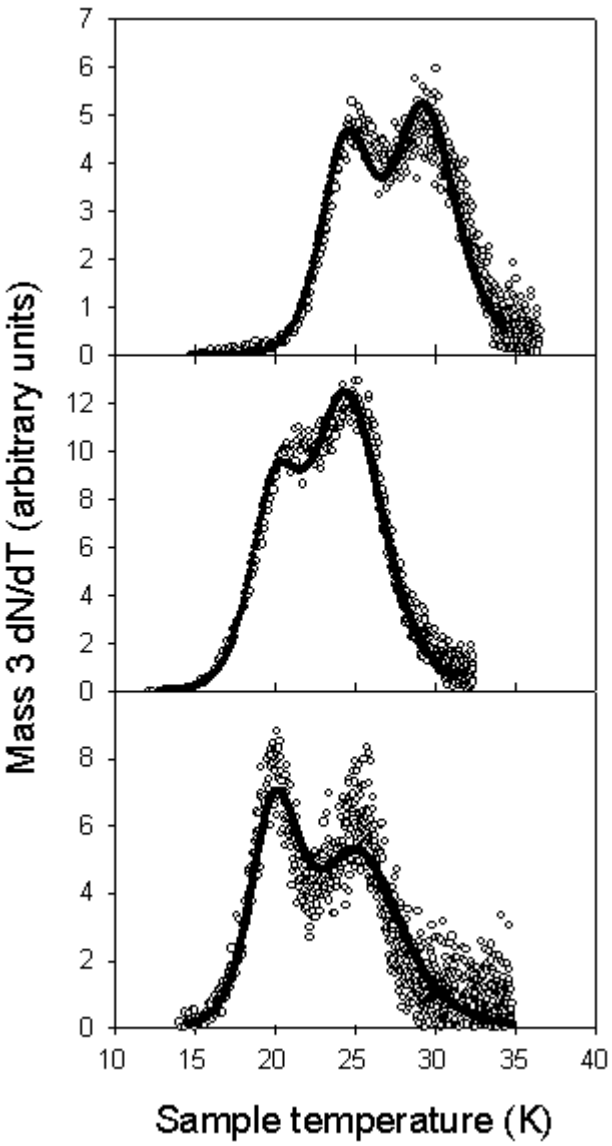

FIG. 6.—Desorption rate (dN_{HD}/dT) vs. ramp temperature after adsorption of H and D for 4 minutes with a sample temperature of ~10 K. Graphs from top to bottom are for desorptions from high-density amorphous ice, low-density amorphous ice prepared by heating a high-density amorphous ice, and water vapor–deposited low-density amorphous ice. The solid line is a fit using the method and parameters described in the text.

yielded information on the order of the kinetics of recombination and desorption (Pirronello et al. 2000). The starting point for the analysis of the TPD traces is the Polanyi-Wigner equation $dN_{HD}(t)/dT(t) = k_m N(t)^m$, where $N(t)$ is the concentration of reactants on the surface, $T(t)$ is the surface temperature during the TPD, m is the order of the desorption, and $k_m = k^{(m)} \exp[-E_a/k_b T(t)]$, with $k^{(m)}$ a constant and E_a an activation energy for the reaction $H_{surface} + D_{surface} \rightarrow HD$ (Vidali et al. 1998). While the temperature of the peaks in a TPD trace depends on the temperature ramp $T(t)$, the activation energies do not; thus, the activation energies give information on the physical processes taking place. Following a careful analysis of the data taken on olivine and amorphous carbon (Katz et al. 1999; Pirronello et al. 1997a), it was found that H and D atoms are set in motion by the temperature ramp of the

TPD, i.e., diffusion is thermally activated. As H and D atoms diffuse, they might encounter each other and form a molecular bond, and the newly formed HD molecule is eventually ejected from the surface. This scenario corresponds, assuming that the desorption is described by the Polanyi-Wigner equation, to a second-order process with $m = 2$. From the analysis of the TPD traces, one can distinguish this scenario from the first-order process with $m = 1$, in which the initial fast mobility of the atoms is due to diffusion by athermal mechanisms. Further indication that HD is not formed right away because of fast H and D mobility comes from the measurement of thermal desorption of H_2 and D_2 from amorphous ice (see Fig. 7). H_2, when adsorbed molecularly at ~5 K, is seen to desorb around 12–14 K, in agreement with the experiments of Rowland et al. (1991). In our experiments in which we adsorb H and D atoms, the bulk of the desorption of HD occurs at temperatures substantially higher than 15 K (see Fig. 6), indicating that molecular hydrogen formation cannot occur because of fast H and D diffusion, or otherwise a substantial amount of HD would leave the surface in times short compared to the laboratory timescale. The fact that a heat pulse must be applied for the reaction to occur and that HD comes off at temperature of 20 K and higher indicates that HD forms via processes of diffusion of H and D activated by thermal energy. Incidentally, our results of H_2 adsorption/desorption are not at variance with the experiments of Watanabe et al. (2000). While our experiment was designed to probe surface or near-surface processes, the experiments of Watanabe et al. involved bulk effects. In one experiment, however, they looked at D_2 adsorption on the ice surface; it was seen that molecularly adsorbed D_2 on amorphous ice came off at a temperature of ~20 K. In that case, however, the adsorption of D_2 occurred at higher temperature than our case, i.e., ~12 K instead of ~5 K; thus, we believe that those authors missed the desorption from the first low-temperature desorption peak and measured the desorption of D_2 coming off from the tail end of the distribution of adsorption sites of D_2 on amorphous ice.

In this study, however, we concentrate our attention on the shape of the desorption trace at a fixed value of the exposure. The presence of broad multipeaked features is due to the fact that there is a range of energies for the reaction $H_{surface} + D_{surface} \rightarrow HD$, which involves the elementary steps of diffusion, molecule formation, and desorption. Computational simulations of amorphous ice surfaces (Buch & Zhang 1991) also demonstrate a heterogeneous energy landscape that is reflected in the activation energies for these elementary steps.

For all three cases presented in Figure 6, we modeled the desorption with desorption kinetics with two discrete characteristic energies. In these cases, it appears that the widths of peaks from the desorption traces are somewhat wider than the peaks produced through the fit, so we modified each fit by integrating each peak with a normalized Gaussian distribution of energies. In this modified fit, we used the functional form $k_m = k^{(m)} \int_{E_p-5\sigma}^{E_p+5\sigma} g(E, E_p, \sigma)^m \times \exp[-E/T(t)]\, dE$ for each peak, where $g(E, E_p, \sigma)$ is a normalized Gaussian distribution of energies E with width parameter σ centered on energy E_p. In adopting this functional form for a distribution of energies, we are assuming two noninteracting adsorbed populations, in addition to assuming that mobility within the energy sites is, within our experimental range of temperature, fast compared to the desorption process. The initial coverage contributing to each peak was determined from a simpler peak fit and was kept constant. The primary effect of including a distribution of energies in our analysis (see Fig. 8) is to widen the calculated desorption peaks to match the experimental traces. Although it is not the aim of this paper to address the issue of the mechanism responsible for the recombination and desorption, we found that the Polanyi-Wigner equation (with the distribution of energy mentioned above) could be fitted to the data more satisfactorily using $m = 2$ (second-order kinetics) than $m = 1$.

From examining Figure 6, it is clear that the middle and bottom panels show traces with similar features, indicating that the two preparation methods, as noted before, yield the same type of ice (low-density amorphous ice). The only visible difference between the two traces is the more visible overlap of the peaks for the heat-treated low-density ice. The peak energies obtained by fitting to the traces are centered at 45 and 68 meV for the heat-treated ice and at 39 and

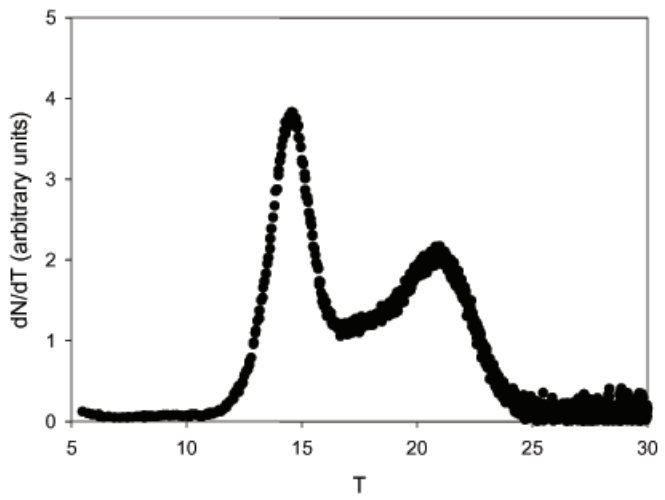

FIG. 7.—Desorption rate (dN_{H_2}/dT) vs. ramp temperature after adsorption of H_2 on low-density amorphous ice for 4 minutes with a sample temperature of ~5 K.

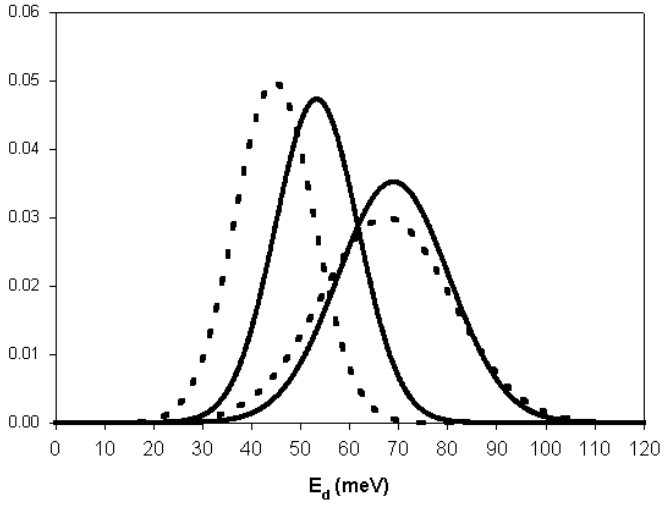

FIG. 8.—Gaussian energy distributions used to fit TPD curves from high-density (*solid line*) and low-density (*dashed line*) amorphous ice samples.

TABLE 1
SUMMARY OF THE RESULTS OF THE FIT TO THE TPD TRACES FOR AMORPHOUS ICE SAMPLES

Amorphous Ice	E1 (meV)	E2 (meV)	w1 (meV)	w2 (meV)
High density	53.4 ± 0.3	69.0 ± 0.2	8.4 ± 0.2	11.3 ± 0.1
Heat-treated low density	44.8 ± 0.2	67.5 ± 0.1	8.0 ± 0.1	13.3 ± 0.1
Vapor-deposited low density	39 ± 2	67 ± 2	3	12.8 ± 0.8

NOTE.—See text for details. The parameters are quoted with the uncertainties resulting from the fit.

67 meV for the vapor-deposited ice. The widths of the Gaussian energy distributions are 8.0 meV for the first peak and 13.3 meV for the second peak for the heat-treated ice, with consistent widths for the vapor-deposited ice. The absolute values are also subject to error because of the uncertainty in evaluating $k^{(m)}$ and N (Vidali et al. 1998) and in knowing the temperature of the sample. Here, $k^{(m)}$ has been estimated to be $\sim 210^{-3}$ cm^2 s^{-1} (see Pirronello et al. 1999), while N is obtained from a coverage versus exposure calibration.

On the other hand (Fig. 6, *top panel*), HD desorption from high-density amorphous water ice shows features that are different from the other two lower traces. The high-temperature ice TPD has a peak at ~30 K that is not present for the lower density ices, while the 20 K feature from the low-density ices in absent from the high-temperature ice. Repeating the fit for this high-density ice TPD spectrum gives peak energies of 53.4 and 69.0 meV; the widths of the Gaussian distributions are 8.4 and 11.3 meV, respectively. In Table 1, we summarize the values of the parameters and their uncertainties.

We cannot identify the specific mechanism for the difference in the energy distributions from a TPD analysis alone. Probably the density of micropores is not the only important factor in determining the yield and energetics of the recombination process. In fact, micropore density should be highest in the vapor-deposited low-density amorphous ice (Stevenson et al. 1999) and relatively low in the heat-treated low-density amorphous ice. This ice has been cycled through the temperature range ~35–40 K, which is close to the threshold temperature for elevated H_2O mobility, as reported in Laufer, Kochavi, & Bar-Nun (1987); however, recombination yield and energetics do not correlate easily with this picture, implying that several aspects of the surface morphology have strong effects on the energy landscape for adsorption and diffusion of both H (or D) and HD.

To measure the effect of UV photons on the ice sample, we proceeded as follows. We first performed a TPD following adsorption of H and D atoms onto an unirradiated ice. We then treated the ice sample with UV radiation before performing a second TPD experiment with the same amount of H and D adsorbed. Each UV exposure was for 15 minutes duration with the same amount of power to the lamp, and multiple UV exposures of an ice sample were alternated with repeated TPD measurements to track the effect of the exposures.

We used a MgF_2 viewport and lens (gradual cutoff from 60% to 0% transmission in the 100–120 nm range). As the threshold for photodissociation of water [$OH(X\ ^2\Pi) + H$ at ~240 nm; $OH(A\ ^2\Sigma^+) + H$ at ~140 nm (Dutuit et al. 1985)] is near the Al_2O_3 cutoff (sharp cutoff from 60% to 0% transmission at ~140 nm), the use of a sapphire viewport would have transmitted a smaller number of high-energy photons for the same flash-lamp power.

We did not observe any qualitative modification of the TPD traces for UV exposures of the low-density amorphous ice. For the high-density ice, 15 minutes of UV exposure through the MgF_2 optics produced an increase in the desorption yield in addition to a change in the TPD spectrum, which can be characterized as moving from the high-density TPD pattern to one resembling the low-density TPD trace. Repeated UV exposures after the initial 15 minutes produced little to no additional change in the TPD traces.

5. ASTROPHYSICAL IMPLICATIONS

Interstellar grains in dense environments constitute by far the most relevant reservoir of ice in the universe, with the high-density amorphous form in greater abundance than the low-density amorphous form or any other form of ice (Jenniskens et al. 1995; Smith, Sellgren, & Tokunaga 1989). The ratio of the abundances of these two forms depends upon the formation processes of the ice layer and its thermal history. The formation of interstellar icy mantles can occur either by the surface reaction of adsorbed O and H atoms or by the deposition (collision, sticking, and accommodation) of water molecules already formed in the gas phase. The formation energy of H_2O via the surface reactions $O + H \rightarrow OH + H \rightarrow H_2O$ is ~1 eV, although whether this would permit the formed water molecules to rearrange themselves into a low-density amorphous structure is unknown.

Experimental data show that below a substrate temperature of ~66 K, deposition of water molecules from the gas phase gives amorphous ice, either in the high-density or low-density form (Jenniskens et al. 1995). Assuming an activation enthalpy of 12 kJ mol^{-1} for a phase transition from high-density to low-density amorphous ice, the first form is always obtained if the substrate temperature is below ~30 K (Jenniskens et al. 1995). Hence, accretion of water molecules on the surfaces of grains in interstellar environments such as dense clouds, where the grain temperature is ~10 K, produces high-density amorphous water ice mantles. This process of formation of high-density ices will be opposed by the transport of material from the "core" of the cloud toward its edge because of turbulence, producing at least a partial conversion to low-density amorphous ice through higher temperatures and higher UV fluxes.

Using the recombination efficiency obtained from our experiments, it is possible to estimate the H_2 formation

rate as a function of the depth inside a dense cloud. In order to perform the desired estimate, we chose the model of Boland & de Jong (1984), because it describes well the abundances of several species observed in small, dense, and cold clouds such as L183 and L134. The model that we use consists of a small, spherical molecular cloud in hydrostatic equilibrium in which both the thermal and turbulent pressures counterbalance self-gravitation. In this model, turbulence is subsonic and the Mach number is the same throughout the cloud. No star formation processes occur, and no internal heat sources are present. In Figure 9, the behavior of density and temperature as a function of depth for the chosen model is shown. In our calculations, we made the simplifying hypothesis that gas and dust are in thermal equilibrium at visual extinctions greater than or equal to 1.

Our estimate of the formation of molecular hydrogen in steady-state conditions is reported in Figure 10 in terms of the rate constant $R(H_2)$ in $cm^3\ s^{-1}$ as a function of the visual extinction for three extreme cases: the case in which the whole mantle of all grains is made of high-density amorphous water ice (*solid line*) and the case in which it is made of low-density ice, obtained either by thermal annealing (*dashed line*) or by water deposition from the gas phase (*dotted line*). The intermediate yields of vapor-deposited low-density water ice can be neglected, especially because the temperature at which such structures form during deposition is too high to have any relevance in dense cold clouds. These estimates are obtained in extreme cases; in reality, the icy mantle on each grain will have a high-density and a low-density component depending on its thermal and irradiation history. The production of molecular hydrogen will be intermediate between the recombination on high-density amorphous water ice and on low-density amorphous ice layers produced by annealing. Two competing processes will regulate the composition of the structure of the grain mantles: (1) the transport of material from the "core" of the cloud toward its edge because of the turbulence that produces annealing of a preaccreted high-density amorphous ice layer by both higher temperatures and higher UV fluxes, and (2) the vapor deposition of water molecules.

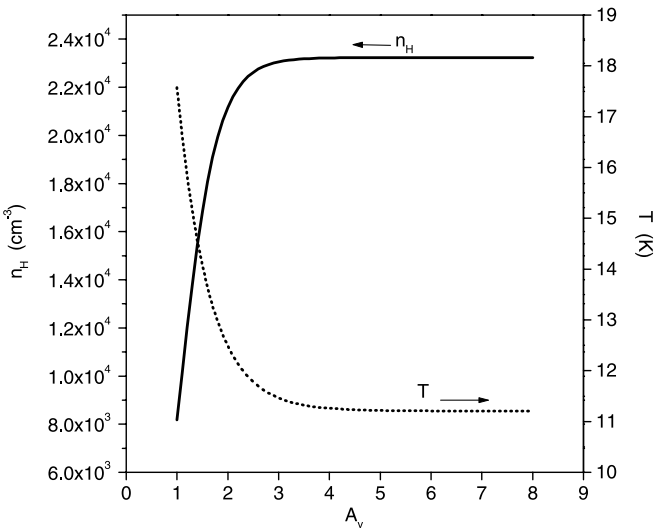

FIG. 9.—Number density and temperature vs. optical depth for the cloud model used in the calculations.

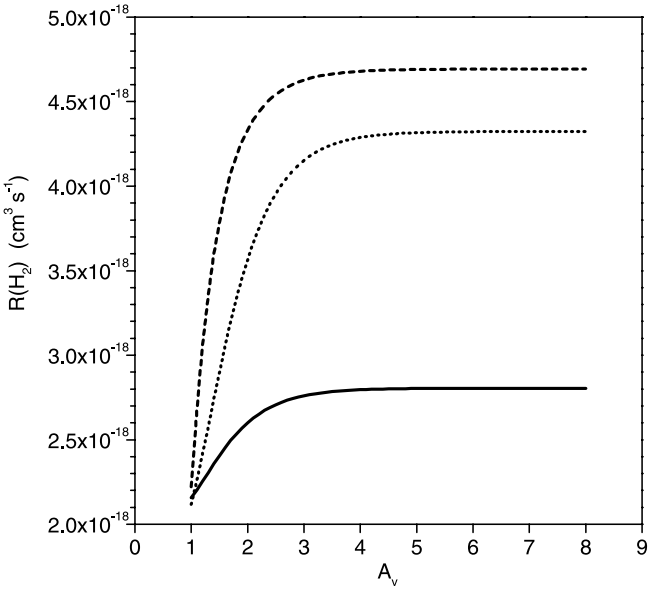

FIG. 10.—Estimated H_2 formation rate constant vs. visual extinction for high-density ice (*solid line*), heat-treated low-density ice (*dashed line*), and vapor-deposited low-density ice (*dotted line*).

Our data show that the recombination efficiency of H_2 is affected from the structure of the ice substrate in which reactions take place, i.e., a high-density amorphous ice sample or a low-density one, the differences being higher when the adsorption temperature is $\sim$10 K and becoming lower and lower as temperature increases (see Fig. 3). Little difference in the recombination efficiency is found between the two methods of producing low-density amorphous ice (vapor deposited or converted from the high-density form by annealing).

As reported previously (Manicò et al. 2001), a recombination efficiency of $\sim$0.35, which is the measured value for high-density ice at $\sim$10 K, can reasonably take into account the production rate of molecular hydrogen in dense clouds at steady state (Manicò et al. 2001). The results of the present paper extend our previous work to both the high-density and the low-density form of amorphous water ice and allow us to say that the fraction of icy mantles in low-density form (converted from high to low density, for instance, by thermal processing) can contribute to the formation of molecular hydrogen with an equal or even higher efficiency than high-density mantles below $\sim$18 K (see Fig. 3).

As a final comment, we would like to point out that TPD spectra of HD (Figs. 4–6) reveal clear differences in the desorption kinetics on the two amorphous icy surfaces. Such differences can be ascribed to differences in both the porosity of the structure and the depth distribution of adsorption wells and almost certainly will affect the energetics of the molecules formed on the surface. Differences due to the amorphous ice structure in the partition of the formation energy between the translational and rovibrational excitation energy carried by formed H_2 molecules may be nonnegligible for interstellar implications. We plan to address this problem after measuring both the kinetic and the excitation energy of just formed molecules.

We acknowledge financial support from NASA to G. V. through grants NAG5-6822 and NAG5-9093. V. P. acknowledges support from the Italian Ministry for University and Scientific Research through grant 21043088. We thank Professor Ofer Biham of the Hebrew University in Jerusalem for helpful discussions, and we thank Robert D'Agostino of Syracuse University for technical assistance in the laboratory.

REFERENCES

Averna, D., & Pirronello, V. 1991, A&A, 245, 239
Boland, W., & de Jong, T. 1984, A&A, 134, 87
Buch, V., & Zhang, Q. 1991, ApJ, 379, 647
Dutuit, O, Tanche-Fouhaile, A., Nenner, I., Frolich, H., & Guyon, P. M. 1985, J. Chem. Phys., 83, 584
Gillett, F. C., & Forrest, W. 1973, ApJ, 179, 483
Gillett, F. C., Jones, T. W., Merrill, K. M., & Stein, W. A. 1975, A&A, 45, 77
Hagen, W., Tielens, A. G. G. M., & Greenberg, J. M. 1981, J. Chem. Phys., 56, 367
Heide, H. G. 1984, Ultramicroscopy, 14, 271
Heide, H. G., & Zeitler, E. 1985, Ultramicroscopy, 16, 151
Hollenbach, D. J., & Salpeter, E. E. 1971, ApJ, 163, 155
Hollenbach, D. J., Werner, M. W., & Salpeter, E. E. 1971, ApJ, 163, 155
Hudson, R. L., & Donn, B. 1991, Icarus, 94, 326
Jenniskens, P., & Blake, D. F. 1994, Science, 265, 753
Jenniskens, P., Blake, D. F., Wilson, M. A., & Pohorille, A. 1995, ApJ, 455, 389
Jones, A. P., & Williams, D. A. 1984, MNRAS, 209, 955
Katz, N., Furman, I., Biham, O., Pirronello, V., & Vidali, G. 1999, ApJ, 522, 305
Kouchi, A., & Kuroda, A. 1990, Nature, 344, 134
Langel, W., Fleger, H.-W., & Knözinger, E. 1994, Ber. Bunsengesch. Phys. Chem., 98, 81
Laufer, D., Kochavi, E., & Bar-Nun, A. 1987, Phys. Rev. B, 36, 9219
Léger, A., Klein, J., de Cheveigne, S., Guinet, C., Defourneau, D., & Belin, M. 1979, A&A, 79, 256
Li, J.-C., & Jenniskens, P. 1997, Planet. Space Sci., 45, 469
Loerting, T., Salzmann, C., Kohl, I., Mayer, E., & Hallbrucker, A. 2001, J. Chem. Phys., 3, 5355
Manicò, G., Ragunì, G., Pirronello, V., Roser, J. E., & Vidali, G. 2001, ApJ, 548, L253
Mayer, E., & Pletzer, R. 1986, Nature, 319, 298
Mishima, O. 1996, Nature, 384, 546
Mishima, O., Calvert, L. D., & Whalley, E. 1984, Nature, 310, 393
Narten, A. H., Vencatesh, C. G., & Rice, S. A. 1976, J. Chem. Phys., 64, 1106
Okabe, H. 1978, Photochemistry of Small Molecules (New York: Wiley)
Pirronello, V., & Averna, D. 1988, A&A, 196, 201
Pirronello, V., Biham, O., Liu, C., Shen, L., & Vidali, G. 1997a, ApJ, 483, L131
Pirronello, V., Biham, O., Manicò, G., Roser, J., & Vidali, G. 2000, in Molecular Hydrogen in Space, ed. F. Combes & G. Pineau de Forets (Cambridge: Cambridge Univ. Press), 71
Pirronello, V., Liu, C., Roser, J. E., & Vidali, G. 1999, A&A, 344, 681
Pirronello, V., Liu, C., Shen, L., & Vidali, G. 1997b, ApJ, 475, L69
Rice, S. A. J. 1975, Topics Curr. Chem., 60, 109
Rowland, B., Fisher, M., & Devlin, J. P. 1991, J. Chem. Phys., 95, 1378
Schmitt, B., Greenberg, J. M., & Grim, R. J. A. 1989, ApJ, 340, L33
Schutte, W. A. 1999, in Laboratory Astrophysics and Space Research, ed. P. Ehrenfreund et al. (Dordrecht: Kluwer), 69
Smith, R. G., Sellgren, K., & Tokunaga, A. T. 1989, ApJ, 344, 413
Smoluchowski, R. 1979, Ap&SS, 65, 29
———. 1981, Ap&SS, 75, 353
———. 1983, J. Phys. Chem., 87, 4229
Stevenson, K. P., Kimmel, G. A., Dohnalek, Z., Smith, R. S., & Kay, B. D. 1999, Science, 283, 1505
Tse, J. 1992, J. Chem. Phys., 96, 5482
van de Hulst, H. C. 1949, Rec. Astron. Obs. Utrecht 11, Pt. II
Vichnevetski, E., Bass, A. D., & Sanche, L. 2000, J. Chem. Phys., 113, 3874
Vidali, G., Pirronello, V., Liu, C., & Shen, L. 1998, Astrophys. Lett. Commun., 35, 423
Watanabe, N., Horii, T., & Kouchi, A. 2000, ApJ, 541, 772
Whittet, D. C. B. 1997, Origins Life Evol. Biosphere, 27, 101